Dynamics of bicontinuous microemulsion phases with and without amphiphilic block-copolymers

M. Mihailescu, M. Monkenbusch, H. Endo, J. Allgaier, G. Gompper, J. Stellbrink, and D. Richter
Institut für Festkörperforschung, Forschungszentrum Jülich, D-52425 Jülich, Germany

B. Jakobs and T. Sottmann
Institut für Physikalische Chemie, Universität zu Köln, Luxemburger Str. 116, D-50939 Köln, Germany

B. Farago
Institut Laue Langevin, Grenoble, BP 156, F-38042 Grenoble Cedex 9, France

(Received 11 July 2001; accepted 31 August 2001)

Neutron Spin Echo and Dynamic Light Scattering techniques are used for an extensive investigation of the bicontinuous phase in water/decane microemulsions. The dynamical behavior of different surfactant systems, decyl polyglycol ether ($C_{10}E_4$), $C_{10}E_4$ mixed with polyethylenepropylene/polyethyleneoxide amphiphilic block-copolymers-(PEP_x/PEO_y), and sodium-bis-ethylhexylsulfosuccinate (AOT) is investigated under comparable conditions. At scattering wave numbers q large compared to the inverse of the structure length scale, $q_0=2\pi/d$, always stretched exponential relaxations $\propto e^{-(\Gamma_q t)^\beta}$ with $\Gamma_q \propto q^3$ are found, as predicted theoretically. The relaxation rate increases almost linearly as function of the bicontinuous structure correlation scale—$\xi \simeq d/2$. The apparent bare bending modulus κ determined by fitting theoretical predictions to the experimental high-q data yields values of about $1.3k_BT$—as inferred from previous small angle neutron scattering (SANS) studies and from other methods. The effect of increasing rigidity of the surfactant layers by anchoring amphiphilic block-copolymers, predicted theoretically and revealed experimentally in structural investigations, could not be clearly resolved due to its small influence on the dynamics. At structural length scales, the relaxation rate in water–oil contrast shows a minimum corresponding to the maximum of the static structure factor. At length scales much larger than the typical structure length the relaxation is single-exponential with a q^2 dependent rate. In this regime we find indications of the additional membrane interaction due to the presence of block-copolymers. © *2001 American Institute of Physics.* [DOI: 10.1063/1.1413509]

I. INTRODUCTION

Mixtures of oil and water are naturally unstable. Adding surfactants such as the commonly used polyglycol-ethers (C_iE_j) leads to microemulsions with a multitude of thermodynamically stable mesoscopic structures which accommodate water and oil with intervening surfactant layers. By variation of physical parameters like temperature, composition, salinity, etc., the system can find preferred aggregation geometries such as globular (droplets of oil in water or water in oil) and bicontinuous, spongelike structures of entangled channels of water and oil, or long-range ordered structures (lamellar, hexagonal, cylindrical) at higher surfactant concentrations.

In the last decades, three main theoretical approaches were developed in order to explain the relative stability of the different phases: microscopic lattice (Ising type) models, phenomenological Ginzburg–Landau models, and effective interface (membrane) models based on the curvature energy of amphiphilic interfaces.[1] An overview of the most recent theoretical developments was given by Gompper and Schick.[2] The increasing interest for the elastic interface approach was due to the fact that, unlike the first two models, it is expressed in terms of physical parameters which can be directly related to experiments. Moreover, it could predict phase diagrams of microemulsions with improving accuracy as the theory has been refined.[3–9]

In the light of the interface model, the richness of the phase diagrams of the surfactant/water/oil systems[10] is caused by a subtle balance between the elastic bending energy of the thermally fluctuating surfactant interfaces, the layer–layer interaction, and the entropy of dispersion. The elastic curvature energy which controls the shape and the fluctuations of the interfaces, is generally written as

$$E_{\mathrm{el}}=\int dS\left[\frac{\kappa}{2}(C_1+C_2-2C_0)^2+\overline{\kappa}C_1C_2\right], \tag{1}$$

where C_1, C_2 are the principal curvatures at each point on the membrane; C_0 is the spontaneous curvature; κ and $\overline{\kappa}$ are the bending rigidity and the saddle-splay modulus, respectively.[1]

Of all the phases, the bicontinuous phase (Fig. 1) is the most intriguing, where by adjusting the temperature and surfactant concentration the optimal emulsification of equal amounts of water and oil can be reached with the least amount of surfactant. Despite its lack of long range order, the regular alternation of water and oil domains in the bicontinuous structure yields a pronounced correlation peak of the scattering intensity at reciprocal space vectors $q_0=2\pi/d$ (where d is the distance between neighbor water–water or

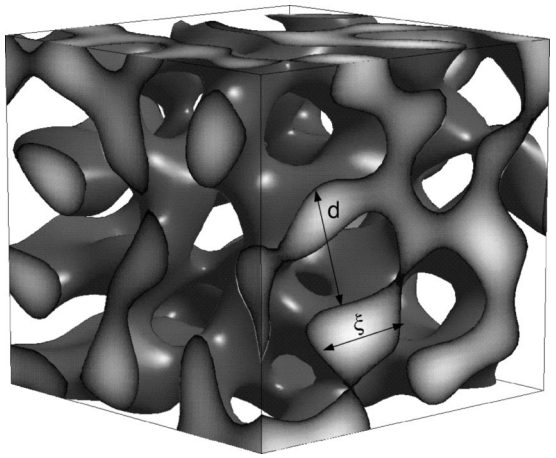

FIG. 1. 3D view of a bicontinuous structure in microemulsion as computed using the level surfaces of a random wave superposition [N. F. Berk, Phys. Rev. Lett. **25**, 2718 (1987)] with parameters chosen for illustration purpose only.

oil–oil domains) in bulk contrast, and a ''shoulder'' at $2q_0$ (corresponding to the surfactant layer–layer distance), in film contrast, as observed by small angle neutron scattering.[11,12]

It was suggested by De Gennes and Taupin[3] that the amphiphilic film is very soft and bends randomly at lengths equal to a characteristic persistence length, ξ_κ, which increases exponentially with the bending modulus, κ. A more detailed analysis of Peliti and Leibler[13] gives $\xi_\kappa \propto \exp(4\pi\kappa/3k_BT)$. It was also shown that the bending modulus can directly be related to the length of the surfactant molecules (i.e., to the alkyl carbon number n, through the relation, $\kappa \propto n^x, x \simeq 2.5$).[14]

Due to a systematic study of the dependence of the optimal (fishtail) point in the phase diagrams on the surfactant molecules type and length, it is now believed that not κ but $\bar{\kappa}$ determines the emulsifying capacity of the surfactants.[15] Recently, the combination of amphiphilic surfactants and polymeric cosurfactants has received much interest. The ''boosting'' effect on the emulsification power of a nonionic amphiphile like $C_{10}E_4$ by block-copolymers (of type PEO_x/PEP_y) addition has been demonstrated in studies of phase diagrams.[16] The corresponding effect on the structure of the bicontinuous phase has been investigated by an extended small angle neutron scattering (SANS) study.[17] Hiergeist and Lipowsky[18] argue that anchoring polymers on an amphiphilic interface would increase its bending modulus κ while decreasing the Gaussian modulus $\bar{\kappa}$, provided that the polymer is evenly distributed on the interface. This is supported by the recent SANS measurements,[17] which reveal decreasing width of the correlation peak with the polymer fraction in surfactant, suggesting an increase of the interface rigidity, and possibly, an enhancement of the repulsive layer–layer interaction.

The question addressed in this paper is how the membrane dynamics at microscopic length scales depends on structure and bending moduli, respectively, how the latter may be inferred from the observed dynamics.

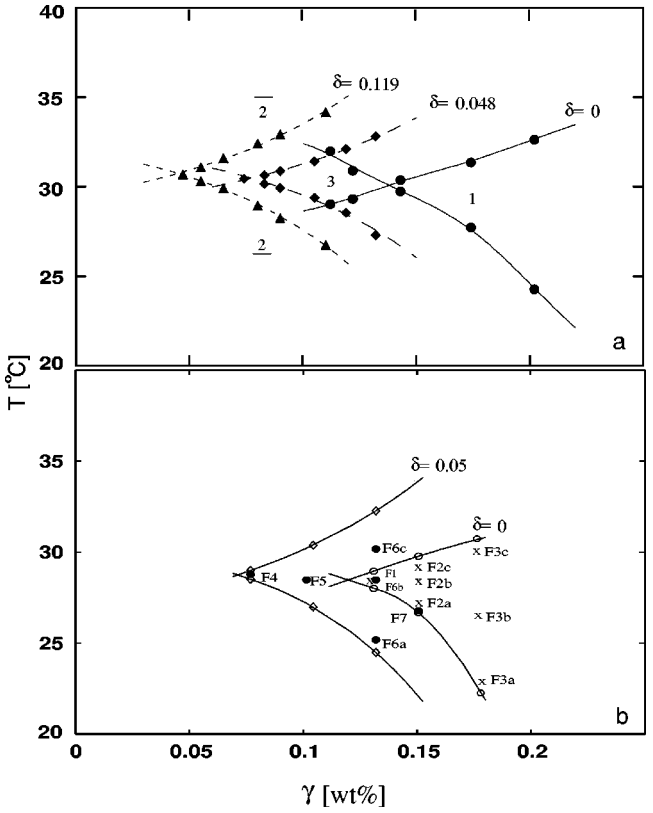

FIG. 2. (a) Phase diagram of h-$C_{10}E_4$/D_2O/h-decane (bulk contrast) and the effect of phase boundary shift due to PEP_{10}-PEO_{10} addition. δ is the weight fraction of polymer in the overall surfactant. (b) Analogous phase diagram with *d*-decane instead of *h*-decane (film contrast). Symbols indicate the actual positions of the investigated systems: ×, no polymer; ●, with polymer.

II. EXPERIMENTS

We performed systematic series of neutron-spin-echo (NSE) experiments and some additional dynamic light scattering (DLS) experiments. In the one-phase bicontinuous region of the phase diagram close to the optimal (fishtail) point the structural size, temperature, and bending moduli (by polymer addition) have been varied. The low-q data have been completed by light scattering results. The effects of variation of the surfactant ($C_{10}E_4$) concentration, i.e., structural length, as well as temperature, and addition of surfactant analogous polymers of different molecular weights have been studied by a systematic series of NSE scattering experiments. The influence of the type of surfactant was investigated using AOT (bis(2-ethylhexyl) sodium sulfosuccinate), an ionic surfactant with bulky hydrophobic part containing two alkyl tails,[19] instead of $C_{10}E_4$, in an analogous phase. All compositions and temperatures were chosen such that the microemulsions were in the bicontinuous phase, not too far from the optimal, ''fishtail'' point (Fig. 2). In case of the AOT, the bicontinuous one-phase was obtained by addition of 0.6% NaCl to the water. The spatial range from 3 nm to 60 nm was explored by neutron scattering and from 300 nm to 1000 nm by DLS.

A. Samples

The microemulsions were prepared by mixing equal amounts (volumes) of oil and water with different amounts

of surfactant—eventually containing polymer. Through our investigation the oil was either *n*-decane ($C_{10}H_{22}$), or deuterated *n*-decane-d_{22} (99%) from Cambridge Isotope Laboratories. Water was used in the form of D_2O (99.95%), supplied by Merck (Germany), or as D_2O/H_2O mixtures in a few cases. The surfactant, $C_{10}E_4$ (tetraethyl-monodecyl-ether) from Fluka (Switzerland), with a purity $>97\%$, was used in its hydrogenated form. All the constituents were used as received. The phase diagram shows a slight shift downwards in temperature upon using deuterated compounds which has been determined by visual inspection in a temperature controlled water bath and accounted for prior to the scattering experiments. We define the surfactant concentration: $\gamma = m_{\text{surfactant}}/(m_{\text{water}}+m_{\text{decane}}+m_{\text{surfactant}})$ and polymeric cosurfactant fraction: $\delta = m_{\text{polymer}}/m_{\text{surfactant}}$, where m_i is the mass of the component "i." Parameter variations like surfactant concentration, γ at constant polymer fraction δ, δ at constant γ, or temperature have been carried out. In the following we will refer to the mixed surfactant system $C_{10}E_4$+PEP–PEO simply as *surfactant*.

B. Added polymers

The amphiphilic block-copolymer used in combination with the $C_{10}E_4$ surfactant were of type polyethylene-propylene-co-polyethyleneoxide (PEP_x-PEO_y), where x and y denote the molecular masses of each of the blocks in kg/mol. The polymers were synthesized by living anionic polymerizations. Details regarding the polymers synthesis process can be found in Refs. 20, 21. In general PEP_{10}-PEO_{10} with the total molecular weight $M_{\text{PEP10-PEO10}} \simeq 21.3$ kg/mol was used in the hydrogenated form. In a few cases the asymmetric PEP_5-PEP_{15} with $M_{\text{PEP5}} \simeq 4.8$ kg/mol and $M_{\text{PEO15}} \simeq 14.1$ kg/mol was studied. The block-copolymers have a structure similar to C_iE_j surfactants, which in the case of PEP_{10}-PEO_{10} can be translated to $C_{715}E_{230}$. The end-to-end distances of the randomly coiled blocks in the respective solvents were estimated from previous light scattering measurements to be 9.7 nm (PEP_{10}), 11.3 nm (PEO_{10}), 6.7 nm (PEP_5), and 13.8 nm (PEO_{15}).[22,23]

C. Scattering contrasts

The huge difference of the scattering lengths[24] of the two stable hydrogen isotopes H and D, $b_{\text{H}} = -3.739$ fm, $b_{\text{D}} = 6.671$ fm allows for an effective selection of the visibility of the different constituents of the microemulsion. In the covered momentum transfer range, $q \leqslant 2\ \text{nm}^{-1}$, the scattering depends only on the average scattering length density,

$$\rho_c = \left\langle \sum_{i\ \text{in}\ j} \frac{b_i}{v_j} \right\rangle_j \tag{2}$$

of the different components c, where i denotes the atoms in molecule j and v_j the molecular volume, and $\langle \cdots \rangle_j$ is the average over the molecules in component c; the scattering length of carbon is $b_{\text{C}} = 6.646$ fm. By selective deuteration (hydrogenation) of the components we are able to observe scattering from either the amphiphilic interface (film contrast) or the difference between solvents (bulk contrast). By very careful contrast variation it is even possible to single out the scattering from the polymeric surfactant component alone.[17] For the present dynamics investigation, however, only film contrast and bulk contrast has been employed. Film contrast was obtained by using *h*-surfactant with D_2O and *d*-decane, whereas bulk contrast samples contained a mixture of D_2O and H_2O with *h*-surfactant and *h*-decane. The reason for choosing the D_2O/H_2O mixture, instead of pure D_2O as one main constituent was the reduction of the very large scattering cross section, which otherwise would have raised concern of multiple scattering. In general, however, sample compositions with low proton and high deuterium content were used to minimize incoherent background and maximize sample transmission. Whereas the salient features of the investigated systems stay unchanged by the isotopic substitution in the course of contrast generation and variation, the temperature of the phase boundaries may shift by several K compared to a fully protonated mixture. However, the topology of the phase diagrams is not effected and the corresponding points relative to the "fishtail" or optimal point are preserved by adjusting the temperature. The phase diagrams for microemulsions prepared on the basis of D_2O are shifted in temperature by about 1.5 K to lower values compared to those with H_2O, whereas microemulsions containing *d*-$C_{10}E_4$, D_2O, and *d*-decane are shifted by about 7 K upwards compared to the microemulsions containing hydrogenous materials. However, the "fishtail" points stay virtually at the same composition γ, independent of the use of deuterated or hydrogenous materials.

D. Investigated microemulsions

The performed scheme of experiments on various microemulsion compositions with the corresponding length scales ξ and d of the bicontinuous structure are listed in Table I. The lengths ξ and d were determined by fitting the Teubner–Strey formula[25] [see Eq. (11) below] to the scattering intensity for a series of SANS measurements (presented elsewhere[17]). The values for the actual concentrations have been obtained by interpolation. The AOT mass fraction $\gamma = 0.124$ was chosen to match the surface per unit volume of $C_{10}E_4$ at $\gamma = 0.13$ since the area per surfactant molecule is different for the two systems ($a_{\text{H}}^{\text{AOT}} \simeq 7.6\ \text{nm}^{12}$ and $a_{\text{H}}^{\text{C}_{10}\text{E}_4} \simeq 5.4\ \text{nm}^{25}$). The phase diagram for the $C_{10}E_4$ microemulsion ($\delta = 0$) and the effect of replacing about 5% ($\delta = 0.048$) and respectively 12% ($\delta = 0.119$) of the surfactant with PEP_{10}-PEO_{10}, for totally hydrogeneous components, is shown in Fig. 2a. The phase diagram corresponding to the actual film contrast compositions is shown in Fig. 2b; the shift in temperature is due to the changed isotopic composition. The numbered positions in the diagram correspond to the compositions listed in Table I, where the symbols are used to identify the microemulsions with polymer (filled circles) and without polymer (crosses), respectively. Since the "fishtail" point shifts towards lower surfactant concentration in the presence of small amounts of polymer, we were able—by adding PEP_{10}-PEO_{10} to the surfactant—to prepare also dilute bicontinuous phases which are, however, only existent in the presence of the block-copolymer. All the investigated systems were prepared within the one-phase region,

TABLE I. Sample compositions.

System	γ	δ	ξ (nm)	d(nm)	Surfactant	Contrast
F1	0.130	0	16.2	32.3		
F2	0.150	0	13.2	26.8	$C_{10}E_4$, no polymer	
F3	0.178	0	7.4	16.2		
F4	0.075	0.050	33.3	61.5		
F5	0.100	0.050	21.3	40.5		
F6	0.131	0.050	16.2	32.3	$C_{10}E_4$	film
F7	0.150	0.050	13.4	27.0	$+PEP_{10}$-PEO_{10}	
F8	0.075	0.077	33.3	61.5		
F9	0.130	0.100	16.7	33.0		
F10	0.130	0.050	16.2	32.3	$C_{10}E_4$ $+PEP_5$-PEO_{15}	
F11	0.124	0	14.4[a]	28.8[a]	AOT	
B1	0.138	0	15.8	31.4	$C_{10}E_4$, no polymer	
B2	0.131	0.050	17.4	34.0	$C_{10}E_4$	bulk
B3	0.133	0.100	17.7	34.8	$+PEP_{10}$-PEO_{10}	
B4	0.138	0.050	15.8	31.4		

[a]Extracted from Ref. 12, where ξ is given for AOT microemulsion at 12% surfactant concentration.

close to the fishtail, at not too high surfactant concentrations in order to stay away from the boundary to the lamellar phase.

The viscosities of the fluids separated by the surfactant layer (Table II) are calculated from the semiempirical formulas for the viscosity variation with temperature of water[26] and decane[27] (see Appendix A). The viscosity parameter required to describe the dynamics of the surfactant membrane in the surrounding fluid is then taken as the arithmetic average of the viscosities of H_2O and h-decane.

TABLE II. Parameters describing the dynamics in film contrast in the high-q limit. On the last column the apparent bending modulus, $\kappa(q=1.6\,\mathrm{nm}^{-1})$ is shown.

System	T(°C)	η_0 10^{-3}[kg/(m s)]	$\bar{\Gamma}=\Gamma_q/q^3$ 10^{-2}(nm^3/ns)	κ/k_BT
F1	28.5	0.82	4.06	1.32
F2a	27.3	0.84	3.59	
F2b	28.5	0.82	3.62	1.20
F2c	29.2	0.81	3.73	
F3a	22.4	0.92	2.66	
F3b	26.8	0.84	3.12	0.50
F3c	30.4	0.79	3.44	
F4	28.8	0.81	5.04	1.84
F5	28.5	0.82	4.55	1.63
F6a	25.2	0.87	3.57	
F6b	28.5	0.82	3.95	1.37
F6c	30.2	0.79	4.22	
F7	26.8	0.84	3.51	1.24
F8	28.3	0.82	4.87	1.86
F9	27.5	0.83	4.06	1.51
F10	28.0	0.82	3.97	1.09[a]
F11	50.2	0.57	6.15	1.09

[a]Corresponding to the maximum $q=1.2\,\mathrm{nm}^{-1}$, measured at IN15.

E. Neutron scattering

The normalized dynamic structure factor $S(q,t)/S(q)$ was determined by neutron spin echo spectroscopy.[28] The Neutron Spin Echo spectrometer in Jülich (NSE-FRJ2) (Ref. 29) was used for most of the presented experiments. Several measurements were also performed at the NSE instrument IN15 at the ILL-Grenoble[30] allowing for extended time range measurements. Custom made (HELLMA), $30\times30\,\mathrm{mm}^2$ rectangular quartz cells (with two Teflon stoppers) of thicknesses 1 mm (for bulk contrast) and 2 mm (for film contrast) were used for the measurements carried out in Jülich. For the NSE experiments they were inserted into a copper frame with quartz windows, thermostated by a water circuit. The temperature difference between the sample cell interior and the thermostated water was corrected for by means of a thermocouple used to correct the set-point for the water temperature. Since the temperature window of the bicontinuous phase was only a few K, the empty cuvettes were inserted into the sample stage and brought to temperature prior to sample injection. At IN15 in Grenoble, a different type of sample cell, consisting of a large copper block containing a middle groove of variable thickness, guarded by quartz windows was used. In all the cases, the freshly prepared microemulsion phase—having the corresponding temperature—was injected *in situ* into the preheated sample cell (cuevette) using a syringe with a Styrofoam thermal insulation. Visual inspection through the quartz windows was performed to ensure that no phase decomposition took place. The standard measuring sequence at the NSE-FRJ2 covered the q-range from $0.3\,\mathrm{nm}^{-1}$ to $2\,\mathrm{nm}^{-1}$ using five different nominal scattering angles, each of which may yield about four different q-values in the area-multidetector range, within a band of $\Delta q=0.6\,\mathrm{nm}^{-1}$.[29] The wavelength used was $\lambda=0.8\,\mathrm{nm}$ with a FWHM of $\Delta\lambda/\lambda=0.1$. The time range covered was $0.1<\tau/\mathrm{ns}<22$. A complete measurement on one sample at one temperature required 12–24 h. In an attempt to enlarge the q-range at the low-q side we used the NSE-FRJ2 in a *small angle configuration*, thus probing the dynamics in a q-regime around the structure correlation peak. For this purpose the incoming beam aperture, at the first $\pi/2$ flipper and also close to the sample position (at a distance of $\approx3.2\,\mathrm{m}$ from the first aperture) were reduced to 2 cm diam. The associated intensity reduction by a factor 10 is acceptable only because the microemulsions scatter very strongly. The scattering angle setting was chosen such that the beam axis hits the area detector off-axis, the primary beam was blocked by a 6 cm diameter beam stop in front of a large area background suppression collimator in front of of the analyzer. By this procedure we could analyze the relaxation curves down to values $q=0.08\,\mathrm{nm}^{-1}$. Because of the—general—slowing down at low q the relaxation effect observable at $\tau_{\max}=22\,\mathrm{ns}$ is small, requiring high counting time (12–24 h) and high instrument stability to be measurable.

At the IN15 the time range up to 166(35) ns has been explored in the q-range $0.15-0.8\,\mathrm{nm}^{-1}$ using wavelengths

TABLE III. Parameters describing the dynamics in bulk contrast in the hydrodynamic limit.

System	T(°C)	η_0 10^{-3}[kg/(m s)]	$\bar{D}_{\text{eff}}$ 10^{-2}(nm^2/ns)
B_1	27.8	0.83	4.86
B_2	28.0	0.82	6.75
B_3	27.5	0.83	7.16
B_4	27.8	0.83	5.31

$\lambda = 1.48(0.88)$ nm with $\Delta\lambda/\lambda = 0.15$ FWHM for a smaller number of samples (i.e., the samples numbered F1, F6b, and F9 in Table II and, respectively B1, B2, and B3 in Table III).

F. Dynamic light scattering

In order to reach the very low-q regime dynamic light scattering (DLS) experiments were performed. An (ALV SP-125/ALV5000E) instrument, using an argon ion laser and operating with vertically polarized light (wavelength in vacuum, $\lambda_0 = 514.5$ nm) was used. The scattering wave vector is given for light scattering by: $q_{\text{DLS}} = 4\pi n \cdot \sin(\Theta/2)/\lambda_0$, with n, the refractive index of the sample [in our case $n_{D_2O} = 1.328$, $n_{\text{decane}} = 1.43$, and $n_{\text{eff}} = (n_{D_2O} + n_{\text{decane}})/2$]. All measurements were performed at 27.5 ± 0.1°C in the angular range $30° \leqslant \Theta \leqslant 150°$ yielding a q-range from 8×10^{-3} to 3×10^{-2} nm^{-1}.

III. THEORETICAL DESCRIPTION

Unfortunately a complete, coherent theoretical description of the dynamics of a bicontinuous microemulsion is not yet available. However, there are a few approaches for the limiting cases of large wave numbers probing mainly local membrane motion and, on the other hand, Ginzburg–Landau-type theories for the regime of q-values below $2\pi/d$.

A. High q dynamics

At large wave numbers q ($q \gg q_0$) we are probing thermally induced layer displacements (undulations) of the impermeable amphiphilic membranes. The driving force is the layer elasticity characterized by the bending modulus κ while the dissipative mechanism is the friction which the layer displacement motions experience due to induced flow of the surrounding solvent. On very local scales (however larger than the molecular size) Zilman and Granek[31] represent the amphiphile layer in the bicontinuous network as consisting of an ensemble of independent patches at random orientation of size equal to the correlation length ξ. The patches are assumed to be locally nearly planar, i.e., $[\nabla_r h(\mathbf{r})]^2 \ll 1$, where $h(\mathbf{r},t)$ describes the local membrane displacement from an average reference plane. The free energy of deformation due to undulation of the patch is approximated by

$$H = \frac{1}{2}\kappa \int d^2r [\nabla_r^2 h(\mathbf{r})]^2 = \frac{1}{2}\kappa \sum_{\mathbf{k}} k^4 h_{\mathbf{k}} h_{-\mathbf{k}}, \tag{3}$$

where $\mathbf{k}$ labels the undulation modes. Expression (3) takes account of the membrane bending only, any interaction effects are ignored. With the assumption of a Gaussian distribution for the variable $[h(\mathbf{r},t) - h(\mathbf{r}',0)]$, and not too large undulations, the structure factor of the membrane is given by

$$S(q,t) \propto \left\langle \int d^2r \int d^2r' e^{i\mathbf{q}_\parallel(\mathbf{r}-\mathbf{r}')} e^{-(q_z^2/2)\langle[h(\mathbf{r},t)-h(\mathbf{r}',0)]^2\rangle} \right\rangle_\alpha, \tag{4}$$

where locally, $q_\parallel$ is the in-plane component of the scattering vector, while q_z is the component perpendicular to the surfactant layer surface. The whole expression of $S(\mathbf{q},t)$ must be averaged over the angle α between the wave vector $\mathbf{q}$ and the local membrane surface normal (see also Appendix B). The fluctuation dynamics (of relaxation type) requires balancing of the forces due to Eq. (3) with friction due to the viscous flow of the embedding fluids. The resulting *membrane Zimm dynamics* yields $\omega(k) = (\kappa/4\eta)k^3$ for the dispersion of the undulation modes,[32,35] and

$$\langle h_{\mathbf{k}}(t) h_{-\mathbf{k}}(0)\rangle = \frac{k_B T}{\kappa k^4} e^{-\omega(k)t} \tag{5}$$

for the membrane displacement correlation, obtained as solution of a corresponding Langevin equation. Note that the mode wave vector $\mathbf{k}$ may not be confounded with the experimental $\mathbf{q}$ vector. Expanding $\langle[h(\mathbf{r},t) - h(\mathbf{r}',0)]^2\rangle = U(\mathbf{r} - \mathbf{r}',t)$ in its Fourier representation, and observing Eq. (5) leads to

$$\begin{aligned} U(\mathbf{r}-\mathbf{r}',t) &= \frac{1}{2\pi^2}\frac{k_B T}{\kappa}\int_{k_{\min}} \frac{d^2k}{k^4}[1 - e^{i\mathbf{k}(\mathbf{r}-\mathbf{r}')}] \\ &\quad + \frac{1}{2\pi^2}\frac{k_B T}{\kappa}\int_{k_{\min}} \frac{d^2k}{k^4} e^{i\mathbf{k}(\mathbf{r}-\mathbf{r}')} \\ &\quad \times [1 - e^{-\omega(k)t}] \\ &= \phi_s(|\mathbf{r}-\mathbf{r}'|) + \phi_d(|\mathbf{r}-\mathbf{r}'|,t) \end{aligned} \tag{6}$$

with the static part $\phi_s(r) \propto r^2 \ln(\xi/r)$, and the dynamic part,

$$\phi_d(r,t) \simeq \frac{k_B T}{\pi\kappa} r^2 F\left(\frac{\kappa t}{4\eta r^3}\right), \tag{7}$$

with the scaling function $F(x) = x$ for $x \to 0$ and

$$F(x) = \tfrac{1}{2}\Gamma(\tfrac{1}{3})x^{2/3} - \tfrac{1}{12}\ln x + \cdots \quad \text{for } x \to \infty. \tag{8}$$

The complete integral Eq. (6) needs a small wavelength cutoff, determined by the most extended mode that fits into one patch ($k_{\min} = \pi/\xi$), since ϕ_s is divergent at $k \to 0$; however no high-k cutoff is necessary.[33,34] As may be inferred from Eqs. (7) and (8) as well as the results given in Ref. 31, $U(\mathbf{r} - \mathbf{r}',t)$ has a leading time-dependence $\propto t^{2/3}$ (for $t \to \infty$) modified by some $|\mathbf{r}-\mathbf{r}'|$ dependent corrective terms. This translates into the stretched exponential dependence given in the limit of large q and large $\kappa \gg k_B T$ by Zilman and Granek as follows:

$$S(q,t) \simeq S(q)\exp(-\Gamma_q t)^\beta, \tag{9}$$

with $\beta=2/3$ and the relaxation rate,

$$\Gamma_q=0.025\gamma_\kappa\left(\frac{k_BT}{\kappa}\right)^{1/2}\frac{k_BT}{\eta}q^3, \tag{10}$$

where, $\kappa=$bending elasticity modulus, $\eta=$solvent viscosity, and $\gamma_\kappa\simeq 1-3(k_BT/4\pi\kappa)\ln(q\xi)\to 1$ for $\kappa\gg k_BT$.[35]

The γ_k factor comprises the effects of angular averaging between **q** and the disk surface normal, within some approximation. A similar expression (without the γ_k factor) should hold for an oriented lamellar system when replacing q by q_z (the wave vector component perpendicular to the lamellar plane). This result for $S(q,t)$ can also be found in the work of Frey and Nelson,[36] as a particular case from a more general approach on the dynamics of membranes. The value of the stretching exponent β is related to the mode dispersion relation for the *membrane Zimm dynamics* $\omega(k)\propto k^3$. Equation (4), for planar plaquettes, preferentially selects contributions along $\mathbf{q}_z$ leading to a time dependence $\propto q_z^2t^{2/3}=(q_z^3t)^{2/3}$ revealing the cause of the q^3-dependence of the rate Γ_q. The q_z projection feature of Eq. (4) results from the fact that the 2D Fourier transform of a platelet is a rod in reciprocal space and that it applies here since the leading time-dependent contribution to $\langle[h(\mathbf{r},t)-h(\mathbf{r}',0)]^2\rangle$ as expressed by ϕ_d, Eq. (7), does not depend on $\mathbf{r},\mathbf{r}'$ for sufficiently large times. In this simplified view the angular averaging does not change the time dependence too much, except replacing q_z by q. Since the denominator of the exponent in the $t^{2/3}$ dependence stems from the exponent of k in the *membrane Zimm dynamics* dispersion relation $\omega(k)\propto k^3$, the (asymptotic) value of β conveys information of the high-k mode dispersion.

The γ_k factor given by Zilman and Granek is only close to 1 if $\kappa\gg 1k_BT$; since bicontinuous phases imply low membrane rigidities, $\kappa\approx 1k_BT$,[2] and from previous SANS studies $\kappa\simeq 0.9$–$1.3k_BT$ is anticipated for our system,[37] the asymptotic expression for γ_k must be replaced by an explicit numerical evaluation of the angular average. The quoted γ_k would otherwise lead to unreasonable, even negative rates. The corresponding scheme—extending the Zilman and Granek procedure—is described in Appendix B and is used in the following data analyses.

B. Intermediate and low-q dynamics

All currently available theoretical approaches, which focus on explaining the dynamical behavior of ternary microemulsions in the range of length scales larger than the typical domain size $d=2\pi/q_0$, are based on Ginzburg–Landau models with two scalar order parameters. These order parameters are $\psi(\mathbf{r},t)$, the local concentration difference of oil and water, and $\rho(\mathbf{r},t)$, the local deviation of the surfactant concentration from its average value. For the investigation of static, structural properties of microemulsions, such a model has first been introduced by Roux *et al.*[38,39] This model works well to explain a characteristic $1/q$-decay of the film scattering intensity for $q\ll q_0$. However, since it assumes a monotonic decay of the oil–oil or water–water correlation function, it fails to produce a peak in the bulk scattering intensity at $q=q_0$ as well as the peak or shoulder of the film scattering intensity at $q=2q_0$. This problem has been cured by Gompper and Schick,[40] by extending the model to oscillating oil–oil or water–water correlation functions. In this case, the bulk scattering intensity is identical to that proposed by Teubner and Strey,[11]

$$S_\psi(q)\propto\frac{1}{q^4-2(q_0^2-\xi^{-2})q^2+(q_0^2+\xi^{-2})^2} \tag{11}$$

which is well known to describe experimental data very well. This represents the Fourier transform of the real-space correlation function, $\langle\psi(r,t)\psi(0,t)\rangle=(1/r)\,e^{-r/\xi}\sin(qr)$ which results from the minimum number of terms with the required symmetry in the free energy $\mathcal{F}$ expansion in terms of ψ and its spatial gradients, which yield a realistic description of $S_\psi(q)$.

The film scattering intensity is calculated to leading order in a perturbative expansion in the coupling constants of the interaction terms between the two order parameters. The resulting scattering functions reproduce all essential features of the experimental scattering data.[17] In particular, from the detailed analysis of the bulk and film structure factors, it is possible to determine the values of most of the coupling parameters of the two-order-parameter Ginzburg–Landau model.

These Ginzburg–Landau models are therefore a promising starting point for a description of the dynamical behavior. The relaxation process in complex fluids proceeds by diffusion and advection. These processes are taken into account by Langevin equations of the form,

$$\frac{\partial}{\partial t}\psi(\mathbf{r},t)=\Gamma_\psi\nabla^2\frac{\delta\mathcal{F}}{\delta\psi(\mathbf{r},t)}+\nabla[v(\mathbf{r},t)\psi(\mathbf{r},t)] \tag{12}$$

and a linearized Navier–Stokes equation for the fluid velocity $v(\mathbf{r},t)$. For the model with the monotonically decaying water–water correlation functions, the dynamic scattering intensities have been calculated by Granek and Cates[41] and by Milner *et al.*[42] The validity of these results is limited to the regime $q\ll q_0$. The model with oscillating correlation functions has been studied by Hennes and Gompper[43,44] and, using a different theoretical technique, by Nonomura and Ohta.[45] We restrict our discussion to the latter model.

The main difference of the analyses of Refs. 44 and 45 for the bulk scattering intensity is the treatment of the hydrodynamic interactions. This is done in a perturbative expansion to one-loop order in Ref. 44, which implies that the effect of the structure on the flow field is omitted to this order in the perturbation theory. The calculation of Ref. 45, on the other hand, is based on an Oseen tensor approach, and takes into account the modification of the flow field. In both cases, the bulk scattering intensity is found to be

$$G_{\psi\psi}(\mathbf{q},t)\propto\exp(-\Gamma_b(q)t) \tag{13}$$

for large t, where the relaxation rate $\Gamma_b(q)$ has the form

$$\Gamma_b(q)=\Gamma_\psi q^2[S_\psi(q)]^{-1}+D(q)q^2 \tag{14}$$

with a diffusion coefficient Γ_ψ of the solvent, $D(q)\propto 1/\eta$, and η the solvent viscosity. The results of Ref. 44 correspond to $D(q)$ being independent of q, while the incorporation of the structural effects on the flow implies[45] (see Appendix C)

$$D(q)=\frac{q_0}{6\pi\eta}N(q/k_0,u/k_0), \tag{15}$$

with the variables $k_0=\sqrt{q_0^2-1/\xi^2}$ and $u=\sqrt{2q_0/\xi}$. The scaling function $N(q/k_0,u/k_0)$ shows a dip at finite wave number $q=k_0$. The qualitative behavior of the relaxation rate, however, is the same in both approximations, with a pronounced minimum at the characteristic wave number (for sufficiently large $q_0\xi$). The origin is the peak of $S_\psi(q)$ at $q=q_0$.

The film correlation function is also described by an exponential decay,

$$G_{\rho\rho}(\mathbf{q},t)\propto\exp(-\Gamma_f(q)t) \tag{16}$$

for large t. The coupling of the two order parameters in the free energy is treated perturbatively in the calculation of Hennes and Gompper.[44] For the case of high amphiphile mobility, which we consider relevant for our microemulsions, various relaxation regimes arise due to the fact that different relaxation times dominate over some range of wave vector. The relaxation in the regime $q<\xi^{-1}$ is found to be dominated by the relaxation rate,

$$\Gamma_f(q)=\tfrac{1}{2}\Gamma_\psi q^2[S_\psi(q/2)]^{-1} \tag{17}$$

while the relaxation rate becomes independent of q in the regime $\xi^{-1}<q<q_0$. With realistic parameters of our system, e.g., $\xi=15.8\,\mathrm{nm}$ and $q_0=0.2\,\mathrm{nm}^{-1}$ (which gives the dimensionless structural parameter $q_0\xi=3.16$), the latter regime is very narrow. We want to mention parenthetically that due to the neglect of the coupling of the order parameters in the free energy in the analysis of Ref. 45, the peak in the static film scattering function is absent, and a simple q^2-dependence is found for balanced systems.

It is important to note that while the behavior at wave vectors $q\gg q_0$ is governed by membrane undulation modes (compare Sec. III A), the dynamical behavior at intermediate wave vectors, near q_0, is strongly affected by topological membrane changes, i.e., the creation and destruction of passages between surfactant monolayers. Such topology changes are contained in the Ginzburg–Landau theories described above.

Our experimental data will be compared to these theoretical predictions in Sec. IV B below.

IV. EXPERIMENTAL RESULTS

A. High q dynamics ($q\gg q_0$)

Figure 3 shows typical NSE experimental relaxation curves collected at FRJ2-Jülich and IN15-Grenoble as obtained from the ternary microemulsion h—$C_{10}E_4$/D_2O/d—decane in film contrast, labeled F1 in Table I. The data from the two instruments and from different sample preparations (of the same nominal composition) show a very good agreement at corresponding wave numbers, q, in the overlapping time range. An analysis in terms of stretched exponentials of the normalized intermediate scattering function, i.e., $S(q,t)/S(q)\simeq\exp[-(\Gamma(q)t)^{\beta(q)}]$ gathered systematically at the FRJ2-Jülich for the systems enumerated in Table I reveals characteristic features of the high-q relaxation. The q^3 dependence of the relaxation rate Γ_q, observed experimentally for bicontinuous and sponge phases and expected theoretically for lamellar systems[46–48] is confirmed, as may be inferred from Fig. 4 where the reduced relaxation rates $\Gamma^*(q)=(\Gamma_q/q^3)(\eta_0(T)/k_BT)$ are shown. The viscosity dependence of the relaxation rate, Eq. (10), was eliminated by multiplication with $\eta_0(T)$, assuming that all the friction effects relate to the average viscosity of oil and water. In the upper part of Fig. 4 the reduced relaxation rates $\Gamma^*(q)$ for different surfactant systems of the same structure size d, are directly compared and seen to coincide on average. The average relaxation rate values $\overline{\Gamma_q}/q^3$ presented in Table II were calculated taking only the data points in the

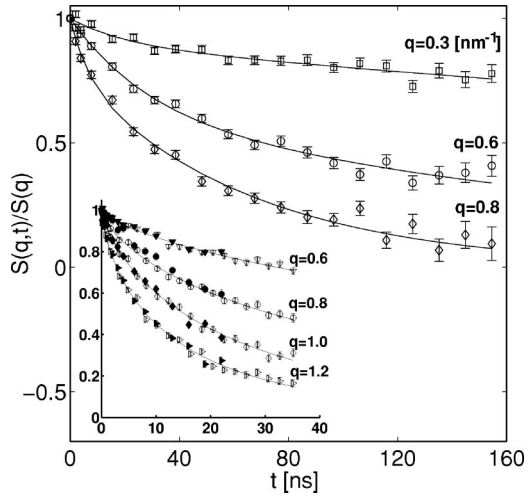

FIG. 3. Experimental relaxation curves measured at IN15-Grenoble (open symbols) and Jülich (full symbols) in the long-time and short-time range (insert). The solid lines show the individual stretched-exponential fit to the data [Eq. (9)], with $\Gamma=\Gamma_q/q^3$ and β as fit parameters.

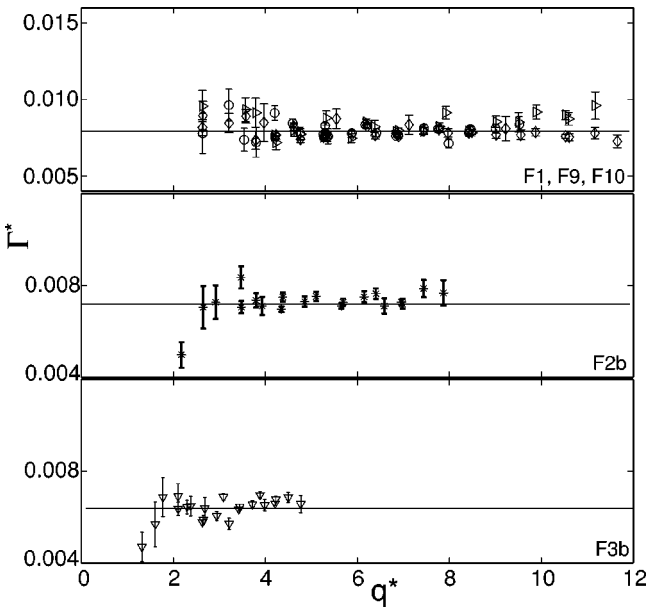

FIG. 4. Reduced relaxation rate $\Gamma^*(q)=(\Gamma_q/q^3)(\eta_0(T)/k_BT)$ vs reduced scattering wave vector $q^*=q/q_0$ for various surfactant types: F1 $\equiv C_{10}E_4$ (○), F9$\equiv C_{10}E_4+PEP_{10}$-$PEO_{10}$ (▷), F10$\equiv$AOT (◇), and respectively, surfactant ($C_{10}E_4$) concentrations: F2b, (*); F3b, (▽).

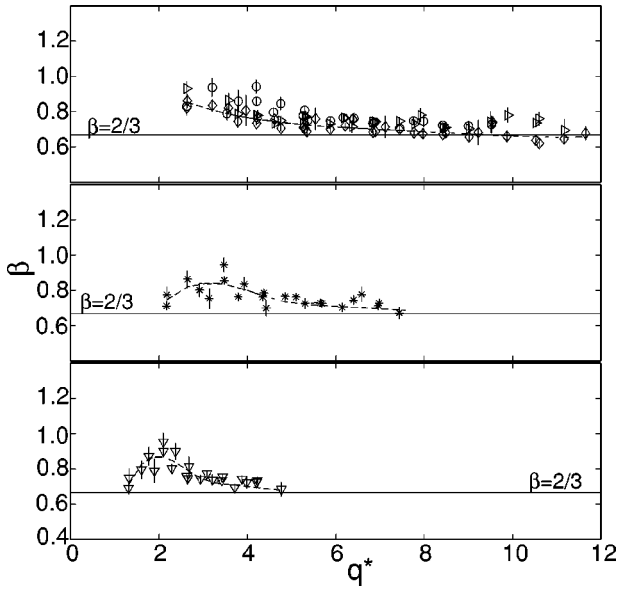

FIG. 5. Exponent β vs reduced scattering wave vector $q^*=q/q_0$ for various surfactant types: F1$\equiv C_{10}E_4$ ($\bigcirc$), F9$\equiv C_{10}E_4+PEP_{10}$-$PEO_{10}$ ($\triangleright$), F10 $\equiv$AOT ($\diamond$), and various surfactant concentrations: F2b, (*); F3b, ($\triangledown$), respectively.

asymptotic ($q^*=q/q_0>4$) regime, where $q_0=2\pi/d$ was determined for every surfactant concentration based on the value of d given in Table I. Figure 5 displays the stretching exponent $\beta(q)$ for the different systems. As it is observed β approaches the value of 2/3 predicted by the theory, Eq. (9), only in the asymptotic high-q regime ($q^*\gg 1$). Still, from the available high-q data ($q>4q_0$) rather an average value of about 0.75 is found with no systematic dependence on microemulsion composition.

In Fig. 6 the influence of the sample temperature on the relaxation rate is shown. The reduced relaxation rate $\overline{\Gamma^*}$, averaged over the asymptotic high-q data points, is almost constant as function of temperature within $\pm 2\%$ from the average value. Considering Eq. (10) the observed

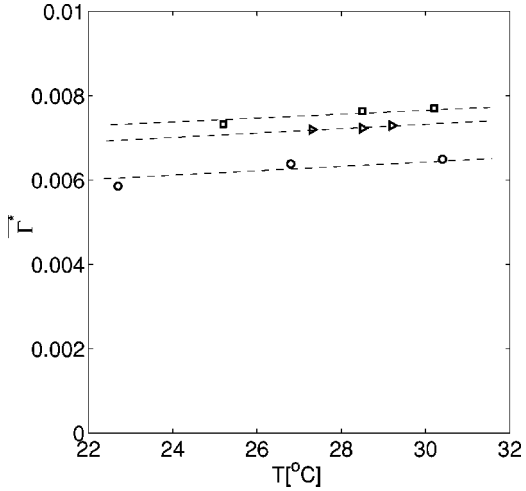

FIG. 6. Average reduced relaxation rate $\overline{\Gamma^*}=\langle(\Gamma_q/q^3)(\eta_0(T)/k_BT)\rangle_{q>4q_0}$ vs sample temperature: F3abc$\equiv C_{10}E_4$ ($\bigcirc$), F2abc$\equiv C_{10}E_4$ ($\triangleright$), and F6abc $\equiv$ $C_{10}E_4+PEP_{10}$-PEO_{10} ($\square$).

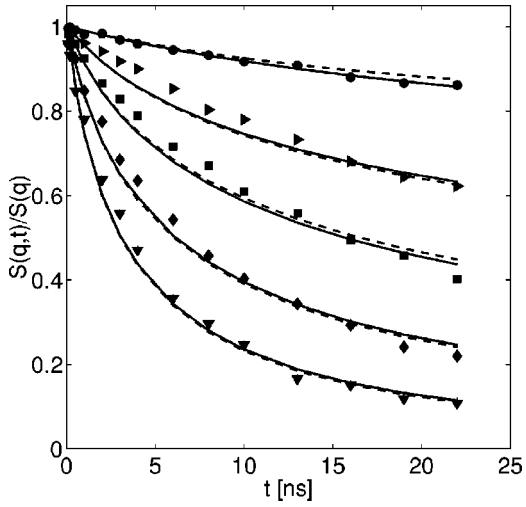

FIG. 7. Fit to the experimental data using numerical procedure [Eq. (B10)] performed individually for each q-value (solid lines), and simultaneously (dashed lines). The curves correspond to the q range from $0.5\,\mathrm{nm}^{-1}$ to $1.6\,\mathrm{nm}^{-1}$.

T-dependence of $\overline{\Gamma}_{q>4q_0}=\overline{\Gamma}_{q>4q_0}(T)$ may be mainly attributed to the temperature dependence of the viscosity $\eta_0(T)$. The weak residual increase of $\overline{\Gamma^*}$ with temperature could be associated with a slight T-dependence of the bare bending modulus κ.

In order to determine the values of the bending modulus κ, we proceed by fitting the experimental data with the dynamic structure factor expression given in Appendix B, Eq. (B10). The only fitted parameter is κ, the viscosity being fixed to the values $\eta_0(T)$ from Table II. In Fig. 7 fits of Eq. (B10) to the full experimental data set are presented. The solid lines are individual fits for each q-value, a simultaneous fit of the decay curves at high q yields the dashed lines in Fig. 7 with a value of $\kappa=1.29\ k_BT$ for the basic system (F1). Values of $\kappa=1.39\ k_BT$ and $\kappa=1.42\ k_BT$ were obtained from simultaneous fits for the systems with polymer (F6) and respectively (F9). In Fig. 8 the apparent values of $\kappa=\kappa(q)$ for systems of equal structural length scale but varying polymer content (F1, F6, and F9) are displayed. As it is observed, except for the lowest-q data point, the values $\kappa(q)$ sit on a roughly constant level around a value of $1.3\ k_BT$ which is in a very good agreement with values of the bare bending modulus found by SANS investigations for this kind of systems.[17] In Table II the apparent bending moduli corresponding to $q=1.6\,\mathrm{nm}^{-1}$ (the highest accessed q for the majority of the systems) are presented. These values should be compared with $\kappa\approx 10\ k_BT$ determined from the stretched exponential fits with Eq. (10) and $\gamma_k=1$. This analysis shows that—at least for very soft, monolayered membranes as presently studied—the asymptotic analytical result [Eq. (10)] cannot be successfully applied.

In any case, in the current analysis we found that there are several sources of uncertainty in determining the bending modulus κ from fits with the integral expression Eq. (B10). The main one is induced by setting the higher cutoff in real space to $r_{\max}\simeq\xi$ and correspondingly, the lower cutoff in the reciprocal space to $k_{\min}\simeq\pi/\xi$ in Eq. (B10).[49] The cutoff at

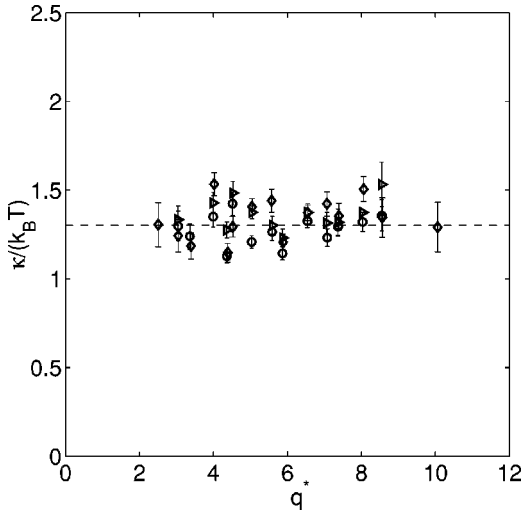

FIG. 8. Values for $\kappa(q)$ as obtained from fits to Eq. (B10) vs reduced scattering wave vector: F1$\equiv C_{10}E_4$ ($\bigcirc$), F6$\equiv C_{10}E_4 + PEP_{10}$-$PEO_{10}$ ($\triangleright$), and F9$\equiv C_{10}E_4 + PEP_{10}$-$PEO_{10}$ ($\diamond$).

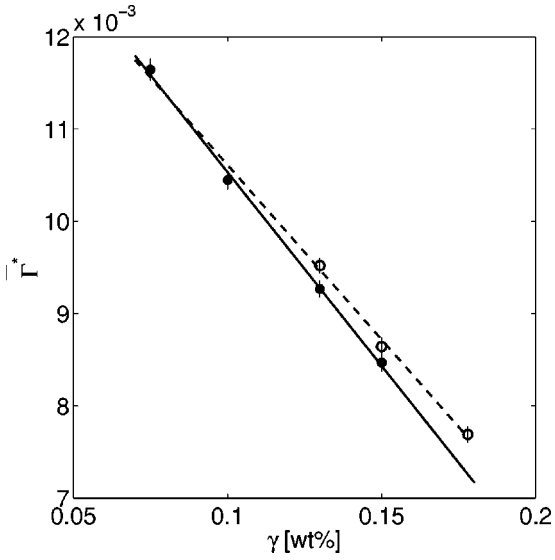

FIG. 10. Average reduced relaxation rate $\overline{\Gamma^*} = \langle (\Gamma_q / q^3)(\eta_0(T)/k_B T) \rangle_{q>4q_0}$ vs surfactant concentration: F1, F2b, F3b$\equiv C_{10}E_4$ ($\bigcirc$), and F5, F6b, F7, F8$\equiv C_{10}E_4 + PEP_{10}$-$PEO_{10}$ ($\bullet$).

$k_{\min}$ is then set consistently by requiring $k_{\min} = \pi/\xi$.

Recent SANS results on microemulsions under film contrast interpreted in the light of Gaussian-random-field models yielded values of $\kappa = 1.2\ k_B T$ for the basic $C_{10}E_4$ system, and respectively, $\kappa = 1.3\ k_B T$ for the system with 10% PEP_{10}-PEO_{10}.[17] Analysis of SANS data in bulk contrast[17,37] yields slightly different values for the bare κ of 0.92 $k_B T$ and 1.23 $k_B T$, for the same two mentioned systems. A value of about 0.8 $k_B T$ can also be estimated for AOT from the structural parameters found in Ref. 12. In order to check for the sensitivity of the results on the exact choice of $k_{\min}$, in Fig. 9 the fitted value of κ is plotted as a function of a calibration factor ϵ which might optimize the cutoff length, i.e., $k_{\min} = \epsilon\pi/\xi$ and $r_{\max} = \xi/\epsilon$, respectively. Having in view the above range of κ values for the different systems, the required scaling factor ϵ is in the range 1.0–1.3 as observed in Fig. 9.

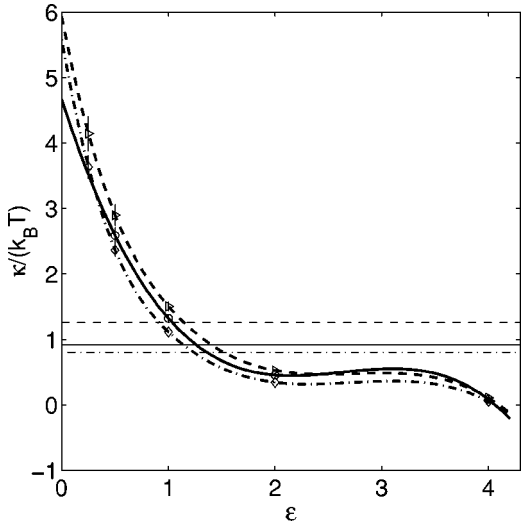

FIG. 9. The apparent κ, from the fits to Eq. (B10), as function of the factor ϵ which scales the integration cutoff $k_{\min} = \epsilon\pi/\xi$, for different systems: $C_{10}E_4$ (full line), $C_{10}E_4 + PEP_{10}$-PEO_{10} (dashed line), and AOT (dash-dotted line). The horizontal lines represent the expected levels of the bending moduli for the corresponding systems, as result from SANS measurements. Symbols indicate the corresponding fitted κ-values.

The most important observed effect on the dynamics correlates to the surfactant concentration, i.e., structural length scale, as shown in Fig. 10. With increasing surfactant content γ, i.e., decreasing structural length scale, the relaxation rate $\overline{\Gamma^*}$ decreases. This effect is large compared to the change due to polymer addition, as observed at iso-structural compositions. The relaxation rate decreases slightly faster with increasing concentration γ when the polymer is present in the membrane.

It is also important to observe that the apparent κ values are significantly different for various surfactant concentrations of the same system as is illustrated in Fig. 11, where results are shown for pure $C_{10}E_4$ systems F1–F3 and systems with 5% polymer content, F4–F7 (compare Table II). Due to the location of the fishtail point, correlation lengths $\xi > 17$ nm are unaccessible in the pure system; only polymer addition allows for values $\xi > 30$ nm where the κ-value seems to saturate. For the pure system, we can only speculate whether the (hypothetical) saturation value would reach the same height or stay lower. Since the influence of the relaxation modes distribution was accounted for by taking the corresponding cutoffs $k_{\min} = \pi/\xi$, the values of κ should not depend on concentration of a specific type of surfactant, i.e., be the same for the three pure system values and, respectively, for the four polymer containing systems. The remaining difference is due to other concentration-dependent effects as it will be discussed in Sec. V.

Henceforth, in order to find the influence of polymer on the membrane dynamics, microemulsions with equal structural length scale but different polymer content were investigated. As we have seen, the results do not show any clear difference in the relaxation rate or exponent β due to the polymer addition and, correspondingly, the variation of κ is

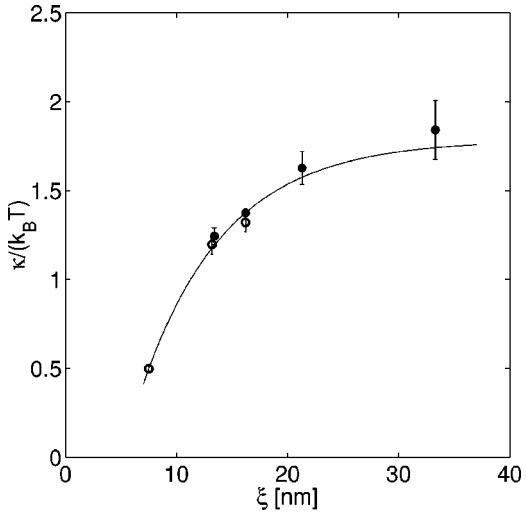

FIG. 11. Apparent (bare) κ vs correlation length ξ, which relates to the surfactant concentration as obtained by fits of the numerically integrated Zilman–Granek expression to the NSE data with $q>4q_0$. Empty symbols: systems F1–F3 containing pure $C_{10}E_4$ as surfactant; solid symbols: systems F4–F7 containing 5% polymer in the surfactant. The line is a guide for the eye only.

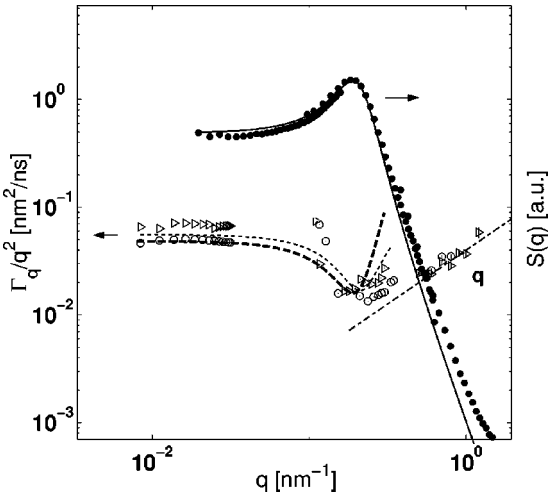

FIG. 12. Effective diffusion coefficient $D_{\text{eff}}=\Gamma_q/q^2$ vs q for $C_{10}E_4+PEP_{10}$-PEO_{10} microemulsion in bulk contrast: without polymer: B1, (○), and with polymer B2, (▷). The dashed and dotted lines reproduce the relaxation rates Γ_b from Eq. (14), and Γ_{11} from Eq. (C3), respectively. The leftmost data sets were obtained by DLS. The dashed–dotted line shows the observed large q-behavior to be proportional to q.

difficult to assess. A discussion of these observations is presented in Sec. V.

B. Intermediate q dynamics ($q \simeq q_0$)

In the analysis of the intermediate q regime the relaxation curves were fitted by a monoexponential function according to Refs. 44, 45. The parameters of proposed Ginzburg–Landau theories related to the structural length scales ξ and d can reproduce the main features of the relaxation rates. However no direct information on the elastic properties of the membranes or the interactions can be inferred. Hence, only a qualitative comparison to our experimental results can be carried out. The intention is to compare systems at the same structural length scale, with or without polymer, in both bulk and film contrasts. Figures 12 and 13 present results corresponding to the pair of systems (B1, B2) in bulk contrast and, respectively, (F1, F6b) in film contrast at $\gamma \simeq 0.13$, and $\delta = 0.05$ whenever polymer is present.

The results on bulk contrast consisting of the low-q regime accessible by DLS and NSE measurements performed in Jülich (for $q \leqslant 0.2\,\text{nm}^{-1}$), and extended for larger q at IN15-Grenoble are gathered in Fig. 12 in terms of Γ_q/q^2. The static structure factor $S_\psi(q)$ corresponding to system B1, determined from the SANS measurements, together with the fit using the Teubner–Strey formula [Eq. (11)] with the parameters $\xi = 15.8\,\text{nm}$ and $q_0 = 0.2\,\text{nm}^{-1}$, are also shown in Fig. 12. The mesoscopic structure of microemulsions is reflected in a minimum of the relaxation rate at $q=q_0$. Using the above structural constants, the effective diffusion Γ_b/q^2 from the Hennes and Gomper approach [Eq. (14)] describes the data reasonably well as shown by the thick dashed line. Moreover, a fit over the low-q region data points (with $q \leqslant q_0$) using the Nonomura and Ohta formulation [Eq. (C3)], where the hydrodynamic contribution $q^2 D_q$ is predominant, yields the thin dashed curve.

In comparison with the bulk contrast, the relaxation rate evolves differently in the case of film contrast as seen in Fig. 13. At low q a q^2 dependence of the relaxation rate is expected according to Refs. 44 and 45. However, the experimental data do not quite cover this regime. In Fig. 13 the relaxation rate Γ_f from Eq. (17) is shown as a dotted line. However, in the interval $0.09-0.2\,\text{nm}^{-1}$ a q-independent relaxation rate is found from the measurements performed at the FRJ2 (the special low-q setup). This feature was predicted qualitatively in Ref. 44 for the range $1/\xi < q < q_0$. A transition to a q^3 regime then occurs at $q=2q_0$ without evidence of a minimum at $q=q_0$. For the so-called "strongly structured microemulsions," which fulfill the condition $q_0\xi$

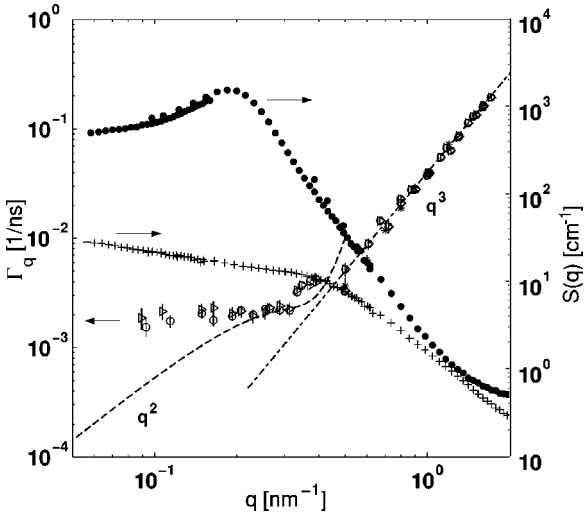

FIG. 13. Relaxation rate Γ_q vs q for $C_{10}E_4+PEP_{10}$-PEO_{10} microemulsion in film contrast at the same surfactant concentration: without polymer F1, (○), and with polymer F6b, (▷). The dashed line reproduces $\Gamma_f(q)$ from Eq. (17). (∗) corresponds to the system F1 measured at IN15 up to 35 ns. (+) and (●) indicate the absolute scattering intensities under film and bulk contrast, respectively.

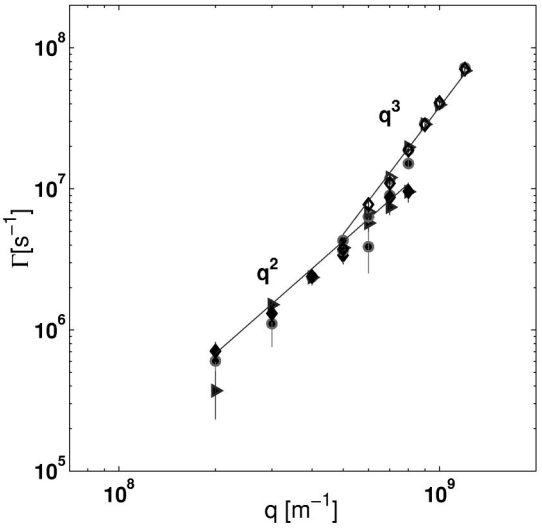

FIG. 14. Relaxation rate Γ_q under film contrast for the systems: F1 $\equiv C_{10}E_4$, without polymer (○), F6b$\equiv C_{10}E_4 + PEP_{10}$-$PEO_{10}$ (▷), and F10 $\equiv C_{10}E_4 + PEP_5$-PEO_{15} (◇), at the same surfactant concentration, measured at IN15 up to 160 ns (full symbols) and 35 ns (open symbols).

>3.5 a minimum in the relaxation rate at $q=q_0$ should also be present according to Ref. 44; however, in our case $q_0\xi \simeq 3$.

Measurements on the pair of systems (F1, F6b) in film contrast were also performed at IN15 for $q \geqslant q_0$, up to $t=166$ ns and for $q \gg q_0$, up to $t=35$ ns, but starting at a somewhat higher minimal q than the data shown in Fig. 13. The larger time range allows here for some rudimentary line shape analysis. The results are collected in Fig. 14 in terms of the relaxation rates. A two-exponential fit of the long time decay curves indicates that the relaxation is not too far from a single exponential with a q^2 scaling (Fig. 14, full symbols) for the lower q values. Comparison with Fig. 13, however, shows that this apparent q^2 behavior rather pertains to a transition region from the high-q q^3-behavior to the regime with constant relaxation rate and is not yet the ultimatively expected simple diffusion regime. Approaching the transition to the q^3 regime, a second, faster component (seemingly q-independent) is contributing to the relaxation; however, due to the large error bars its detailed q-dependence cannot be extracted. The high-q regime was treated in terms of stretched exponentials (open symbols) and the relaxation rates compare very well with the data obtained in Jülich as can be seen also in Fig. 3 and Fig. 13.

C. Low q dynamics ($q \ll q_0$)

The large scale dynamics was investigated by the Dynamic Light Scattering technique. The same composition of microemulsion as presented in Table I for bulk contrast were considered for this purpose with the only difference that all the three samples were measured at 27.5 °C. In the analysis we used the classical cumulant expansion of the intermediate scattering function, $g^{(1)}(q,t)=\exp[-\Gamma_q t+\mu_2/2!\, t^2+\cdots]$,[50] where the mean relaxation frequency $\Gamma_q=\bar{D}_{\text{eff}}q^2$ yields the diffusion coefficient $\bar{D}_{\text{eff}}$. We find nearly monoexponential behavior ($\mu_2 \simeq 0$) for the intermediate scattering function over the whole q-range, with $\Gamma_q \propto q^2$. This suggests a dynamics governed by collective translational diffusion modes of the solvent over space scales much larger than the typical structure length. Unlike the DLS observation in Ref. 51 of two decays in a sodium dodecylsulfate (SDS)/octanol/octane/brine system exhibiting besides the diffusive a second slow relaxation attributed to thermally activated topological changes our system shows only one—diffusive—relaxation. There are other reports of monoexponential as well as nonexponential relaxation for the bicontinuous phase.[52,53] The relaxation rates Γ_q/q^2 determined from this analysis are shown in Fig. 12 together with the NSE results for the system B1 and B2. The determined effective diffusion coefficient values are presented in Table III. It is observed that, in contrast to the minute effect of the polymer on the relaxation rate at high-q, the effective diffusion is significantly larger for the higher polymer density on the membrane surface. The slightly higher surfactant concentration of system B1 can only partly explain the diffusion rate difference. In order to check how much the surfactant concentration contributes to the observed effect upon $\bar{D}_{\text{eff}}$, the sample B4 with polymer, at the same surfactant concentration as the basic system B1, was measured by light scattering. The determined diffusion coefficient is still higher than that for the basic system, without polymer. Considering the solvent flow only, it would be somewhat counterintuitive that the effective diffusion is increasing with the polymer density since the polymer coils extending into the solvent are expected to hinder the solvent flow for the same structural length scales. Therefore, we speculate that the observed enhancement of the relaxation rate results from an increased repulsive osmotic interaction between adjacent membranes due to the presence of polymers anchored to the interfaces.

V. DISCUSSION

First we have shown that the values of κ derived from the final analytic expression given in Ref. 31, with $\gamma_k=1$ are nearly one order of magnitude too high. The modification of this result by explicit numerical integration with the most natural choice of $k_{\min}=\pi/\xi$ for the long-wavelength cutoff of the mode spectrum on a plaquette yield values of $\kappa \simeq 1.3\, k_BT$ for the bare bending modulus in consistency with previous SANS results.[17] The q regime where this analysis seems to be valid is $q^*>4$. There, also the q^3 dependence of the relaxation rate and the stretching exponent $\beta=2/3$ show a good agreement with the predictions of Ref. 31, which becomes better for higher q. At lower q, displacements of regions containing several plaquettes become progressively dominant and other modes besides the undulation mode of the single plaquette must contribute with increasing amplitude to the relaxation.

Secondly, we found that in general, the relaxation slows down with increasing surfactant concentration, i.e., decreasing structure size. Even after taking into account the structural dimension by using $k_{\min}=\pi/\xi$ in the evaluation of Eq. (B10), considerable residual concentration dependence remains in the fitted κ-values (see Fig. 11).

In Eq. (4) the effect of structural cell size on the relax-

ation due to undulation modes is introduced into the dynamic structure factor formulation by taking the appropriate cutoffs as discussed above in Sec. IV. Through this all undulation frequencies which might contribute to the relaxation are integrated. In the high-q regime, the bending modes are probed at short length scales; renormalization effects should therefore be small, so that the measured value of κ can be identified with the bare bending modulus. The bare bending modulus κ should only depend on the surfactant nature and not on the concentration. The residual γ dependence of $\overline{\Gamma}^*$ points to further influences. These may be related to the space available for fluid flow. Since the film dynamics is actually governed by the flow of the solvents on both sides of the membrane, this could simply indicate that with associated decreasing length scale the flow channels are narrowing and the friction associated to the viscous solvent flow increases.

A further observation is that we do not find a significant difference in the dynamics at local scale due to polymer addition relative to the pure $C_{10}E_4$ system (Fig. 4). It is important to mention that at the polymer concentration considered we are in the so called ''mushroom'' regime (i.e., polymer coils do not overlap along the membrane). For the highest polymer concentration the distance between PEP-PEO connection points on the surfactant layer is $\simeq 18$ nm while the end-to-end distance of the blocks is $\simeq 10$ nm for PEP_{10} and $\simeq 11$ nm for PEO_{10}.

Hiergeist and Lipowsky[18] argue that, for a number density of polymer σ in the membrane, the effective bare bending modulus of the layer should be locally increased by an amount $\Delta\kappa=(k_BT/12)(1+\pi/2)\sigma(R_{\mathrm{PEP}}^2+R_{\mathrm{PEO}}^2)$, where $R_{\mathrm{PEP}}, R_{\mathrm{PEO}}$ represent the mean end-to-end distances of the two polymer blocks. Experimentally, from SANS measurements on the same type of systems[37] the slope of this increase was found to be slightly higher, namely, a κ increase from $0.92\,k_BT$ to $1.23\,k_BT$ was found when $\sigma(R_{\mathrm{PEP10}}^2+R_{\mathrm{PEO10}}^2)$ increases from 0 to 0.928. In any case, these small changes in κ would be difficult to detect and discriminate from other effects in the present dynamics experiments.

The fact that the polymer effect—in terms of increase of κ—is less than expected for concentrations where both pure and polymer systems are existent may also result from flow friction effects. Polymers extending into a significant part of the solvents is expected to increase the flow friction and thereby may partly compensate polymer effects on the membrane elasticity. Also the slight difference in the slope of $\overline{\Gamma}^*$ vs γ (Fig. 10), might be attributed to a local increase in the layer–solvent or layer–layer friction due to the presence of polymers.

In general, the here observed concentration dependence of Γ respectively κ is consistent with reports of concentration independent relaxation for very dilute sponge (two-component) systems,[46] if the leveling off of the apparent κ-value at large ξ indicated in Fig. 11 is real.

A much larger influence of polymer addition is observed in the hydrodynamic limit by light scattering studies (Table III). We can see from the values of the diffusion coefficient that the higher the density of the polymer in the interface, the faster the hydrodynamic relaxation. This may be explained by larger layer interactions mediated by the polymers, i.e., a larger compression modulus due to osmotic polymer interactions. These are dominant at low k, where the distinction of k and q vanishes, whereas the κ-dependent terms are proportional to k^4 and dominate at high q.

A direct access to the interface dynamics analogous to film contrast using DLS would require a refractive index matching between water and oil which is not possible without significant changes of the physicochemical properties of either water or/and oil. The crossover regime between the diffusive behavior at very low q (DLS) and the $\Gamma_q \propto q^3$ regime could partly be observed by NSE and it exhibits a kind of ''De Gennes narrowing'' for the bulk contrast dynamics, i.e., $D_{\mathrm{eff}}=D_0/S(q)$.[50,54] The salient features of the q-dependence of the relaxation rate $\Gamma(q)$ for bulk and film contrast are explained by the dynamic versions of Ginzburg–Landau (GL) theories.[44,45] However, there is no method available yet to correlate membrane properties, layer–layer interactions, or flow resistances to the corresponding GL parameters.

VI. CONCLUSION

Optimal emulsification of equal amounts of oil and water with the least amount γ^* of surfactant is achieved at the so-called ''fishtail''-point of the phase diagram of microemulsion systems. At the temperature of the ''fishtail'' point the spontaneous curvature of the interface crosses the zero line, thus in the vicinity of this point the structure of the microemulsion is that of a random bicontinuous network; the typical structural scales d and ξ grow with decreasing γ.[55,56] Addition of polymers which may be considered as macromolecular analogs to the surfactant molecules leads to a drastic shift of the ''fishtail'' point towards lower surfactant contents.[16,17] The boost in emulsification power by this polymer addition has been attributed to changes in the membrane moduli κ and $\overline{\kappa}$. These changes are effected by the decoration of the membrane with polymer ''mushrooms.'' [18] However, since the influence of κ, $\overline{\kappa}$ on the structure and phase behavior is exponential[3,15] the needed κ variations are small.

In the present paper the dynamics of the microemulsion in its bicontinuous phase and the influence of polymer addition has been investigated with the motivation to provide an independent measurement of the bending modulus as a function of polymer content. Especially at larger wave vectors where it may be expected that local membrane properties determine the scattering signal it was expected that the Zilman–Granek expression holds and can be used to extract κ. However it soon turned out that other parameters than the polymer content, in particular the structural size, i.e., the surfactant content, have a much larger influence on the relaxation rate. To enable any comparison, careful systematic studies of the relaxation rate dependence on structural size and temperature for systems with and without polymer had to be performed. Their main result was the observation that for isostructural systems (same d and ξ as realized by choosing the appropriate surfactant concentrations) the relaxation rates are very similar for systems with and without polymer or for different surfactants, e.g., $C_{10}E_4$ or AOT.

Concerning the predicted shape and q-dependence of the relaxation functions the Zilman–Granek analytical result performs well. The stretched exponential behavior of the relaxations with a stretching exponent $\beta \simeq 2/3$ and a q^3 proportionality of the relaxation rate—as expected for *membrane Zimm dynamics*—is observed with fair agreement. Closer inspection, however, leads to the conclusion that full applicability of this theory is only achieved at the upper limit or even beyond the upper limit of the q-range of our observations. At lower q, $\beta(q)$ is significantly larger than 2/3, but it approaches 2/3 slowly with increasing q. It may be concluded that the range of full validity of the Zilman and Granek theory is given only in the asymptotic q-regime. Besides that, we have shown that reliable determination of κ, i.e., consistent with previous experiments, can be achieved only by using the explicit integral expression of $S(q,t)$ with the appropriate cutoffs.

In the intermediate q-regime where the peak due to the structural length is included the only available theoretical predictions are derived from time-dependent Ginzburg–Landau theories,[44,45] which have two concentration fields as constituents of the system. These theories describe the qualitative features of the relaxation rate $\Gamma(q)$ and of the effective diffusion $D_{\text{eff}}(q)$ reasonably well. Especially the scaling by $S(q)^{-1}$ is observed in the bulk contrast scattering. In this regime the relaxation functions are expected to be simple instead of stretched exponentials and the data evaluation is performed under this assumption. However a decay function shape analysis is not possible at very low q, where the total observable decay amounts only to a few percent. Nevertheless it has been achieved to narrow the gap between light scattering and NSE down to only half a decade.

In the light scattering regime a simple diffusive ($\Gamma \propto q^2$) behavior with monoexponential relaxation functions has been observed. The results are to be compared with bulk contrast neutron data, a film contrast analogous light scattering is not available because a refractive index matching of water and decane would be needed. In contrast to the high q-data, the DLS results exhibit a pronounced enhancement of the relaxation on polymer addition. This may be attributed mainly to additional restoring forces due the osmotic pressure of polymer segments that even overcompensate increased friction due to polymers extending into the fluids. Since membrane bending effects scale with k^4, whereas compressibility effects are $\propto k^2$, the latter influences gain relative importance at very low $q \simeq k$.

The present work shows the advantages and limits of the analysis of (membrane) fluctuation dynamics in bicontinuous microemulsion over a large q-range. The extraction of physical parameters as membrane elasticities, interactions, and frictions is still problematic due to the lack of concise theoretical descriptions that are fully valid in the accessible q-regime and depend directly on the physical parameters of interest. A theory that would account for the bicontinuous structure and its influence on fluid flow and membrane modes in combination with the now available data of high statistical accuracy should enable us to extract more detailed parameter values, as the asymptotic behavior of the presently available theory suggests.

APPENDIX A: TEMPERATURE DEPENDENCE OF SOLVENT VISCOSITIES

The semiempirical formulas describing the variation of the viscosities of H_2O (Ref. 26) and decane[27] with the temperature $T[^\circ\text{C}]$ are given by

$$\eta_{H_2O} = 1.002 \times 10^{(1.3272(20-T) - 0.001053(T-20)^2)/(T+105)}[cp], \tag{A1}$$

$$\eta_{\text{decane}} = 8.65 \times e^{1370/(T+273.15)} \times 10^{-3}[cp]. \tag{A2}$$

APPENDIX B: DYNAMIC STRUCTURE FACTORS OF THE HIGH-Q REGIME

The general dynamic structure factor expression for a membrane patch can be written,

$$S(q,t) \propto \left\langle \left\langle \int d^2r \int d^2r' e^{i\mathbf{q}_\parallel(\mathbf{r}-\mathbf{r}')} e^{iq_z[h(\mathbf{r},t)-h(\mathbf{r}',0)]} \right\rangle \right\rangle_\alpha . \tag{B1}$$

The statistical averaging acting on the last exponential factor is solved in terms of cumulant expansion to give

$$S(q,t) \propto \left\langle \int d^2r \int d^2r' e^{i\mathbf{q}_\parallel(\mathbf{r}-\mathbf{r}')} e^{-q_z^2\langle[h(\mathbf{r},t)-h(\mathbf{r}',0)]^2\rangle} \right\rangle_\alpha . \tag{B2}$$

Using the following properties of the Fourier transforms,

$$h(\mathbf{r},t) = \frac{1}{2\pi^2} \int d\mathbf{k} e^{i\mathbf{kr}} h_{\mathbf{k}}(t), \tag{B3}$$

$$h^*_{\mathbf{k}}(t) = h_{-\mathbf{k}}(t), \tag{B4}$$

$$\langle h_{\mathbf{k}}(t) h_{\mathbf{p}}(0)\rangle = (2\pi)^2 \delta(\mathbf{k}+\mathbf{p}) \langle h_{\mathbf{k}}(t) h_{-\mathbf{k}}(0)\rangle, \tag{B5}$$

$$\langle h_{\mathbf{k}}(t) h_{-\mathbf{k}}(0)\rangle = \frac{k_B T}{\kappa k^4} e^{-\omega(k)t}, \tag{B6}$$

and expressing $U(\mathbf{r}-\mathbf{r}',t) = \langle[h(\mathbf{r},t)-h(\mathbf{r}',0)]^2\rangle$ in its Fourier components, the expression (B2), becomes

$$S(q,t) \propto \left\langle \int d^2r \int d^2r' e^{i\mathbf{q}_\parallel(\mathbf{r}-\mathbf{r}')} e^{-1/(4\pi^2)(k_BT/\kappa)q_z^2 \int_{k_{\min}}^{k_{\max}} dk\, 1/k^4 [1 - e^{i\mathbf{k}(\mathbf{r}-\mathbf{r}') - \omega(k)t}]} \right\rangle_\alpha . \tag{B7}$$

In general,

$$\int d^2r e^{i\mathbf{kr}} = \int_0^\infty \int_0^{2\pi} d\phi\, dr\, r\, e^{ikr\cos(\phi)} = 2\pi \int dr\, r\, J_0(kr), \tag{B8}$$

where J_0 is the Bessel function of order 0. Since the membrane patches are randomly oriented with respect to the scattering vector **q**, we have an isotropic distribution of angles α in the interval $0-\pi$ between the normal to the patch and vector **q**,

$$g(\alpha)=\frac{d\Omega}{4\pi}=\frac{2\pi\sin(\alpha)d\alpha}{4\pi}=\frac{1}{2}d\cos(\alpha). \tag{B9}$$

Replacing Eq. (B8) in Eq. (B7) and applying the angular distribution (B9), the expression for the dynamic structure factor used in the fitting procedure is written finally

$$S(q,t)=\frac{2\pi\xi^2}{a^4}\int_0^1 d\mu\int_0^{r_{\max}} dr\, r\, J_0(qr\sqrt{1-\mu^2}) \times e^{-k_BT/(2\pi\kappa)q^2\mu^2\int_{k_{\min}}^{k_{\max}}dk\,[1-J_0(kr)e^{-\omega(k)t}]/k^3}, \tag{B10}$$

where μ is the cosine of α, the angle between **q** and the surface normal.

APPENDIX C: DYNAMIC STRUCTURE FACTORS OF THE LOW-*Q* REGIME

The results found by Nonomura and Ohta[45] for the bulk and, respectively, film dynamic structure factors can be summarized in the following:

$$S_{11}(q,t)=[(1-f)e^{-\Gamma_{11}(q)t}+fe^{-\Gamma_{22}(q)t}] \tag{C1}$$

and

$$S_{22}(q,t)=[fe^{-\Gamma_{11}(q)t}+(1-f)e^{-\Gamma_{22}(q)t}] \tag{C2}$$

with the decay rates of the relaxation,

$$\Gamma_{11}=l_{11}q^2[\chi_\psi(q)]^{-1}+q^2D_q, \tag{C3}$$

$$\Gamma_{22}=l_{22}q^2. \tag{C4}$$

The static correlation function $\chi_\psi(q)$ can be written alternatively,

$$\chi_\psi(q)=\frac{1}{(q^2-k_0^2)^2+u^4}. \tag{C5}$$

Comparing Eq. (C5) to Eq. (11), one can identify $k_0^2=q_0^2-\xi^{-2}$ and $u^2=2q_0\xi^{-1}$. The slower component (Γ_{11}) is associated with the bulk relaxation while the faster one (Γ_{22}) with the film. The off-diagonal part of the Onsager coefficients L_{12}, L_{21} are vanishing when $\overline{\psi}=0$ (i.e., $\overline{\phi}_{\text{oil}}=\overline{\phi}_{\text{water}}$) and the relative friction coefficients $\zeta_{\text{oil/surfactant}}\simeq\zeta_{\text{water/surfactant}}$ and so is the weighting factor defined by $f=\Gamma_{12}\Gamma_{21}/(\Gamma_{22}-\Gamma_{11})^2$. In these conditions, the dynamics structure factors given by Eqs. (C1) and (C2) are reduced to single exponentials. The function D_q mentioned in Sec. III B is written,[45]

$$D_q=\frac{k_0}{6\pi\eta}N(q/k_0,u/k_0), \tag{C6}$$

where

$$N(x,y)=\frac{3\sqrt{2}}{8}\frac{(x^2-1)^2+y^4}{y^2}\int_0^\pi d\theta\sin^3\theta \times\left[\frac{[(x^2\sin^2\theta-1)^2+y^4]^{1/2}+1-x^2\sin^2\theta}{(x^2\sin^2\theta-1)^2+y^4}\right]^{1/2}. \tag{C7}$$

[1] W. Z. Helfrich, Z. Naturforsch. C **28**, 693 (1973).
[2] G. Gompper and G. Schick, in *Phase Transitions and Critical Phenomena*, edited by C. Domb and J. Lebowitz (Academic, London, 1994), Vol. 16.
[3] P. G. De Gennes and C. Taupin, J. Phys. Chem. **86**, 2294 (1982).
[4] S. A. Safran, D. Roux, M. E. Cates, and D. Andelman, Phys. Rev. Lett. **57**, 2718 (1986); D. Andelman, M. E. Cates, D. Roux, and S. A. Safran, J. Chem. Phys. **87**, 7229 (1987); M. E. Cates *et al.*, Europhys. Lett. **5**, 733 (1988).
[5] L. Golubović and T. C. Lubensky, Europhys. Lett. **10**, 513 (1989).
[6] L. Golubović, Phys. Rev. E **50**, R2419 (1994).
[7] D. C. Morse, Phys. Rev. E **50**, R2423 (1994).
[8] G. Gompper and D. M. Kroll, Phys. Rev. Lett. **81**, 2284 (1998).
[9] U. S. Schwarz, K. Swamy, and G. Gompper, Europhys. Lett. **36**, 117 (1996).
[10] M. Kahlweit *et al.*, Langmuir **5**, 305 (1989).
[11] M. Teubner and R. Strey, J. Chem. Phys. **87**, 3195 (1987).
[12] S.-H. Chen, S.-L. Chang, and R. Strey, J. Chem. Phys. **3**, 1907 (1990).
[13] L. Peliti and S. Leibler, Phys. Rev. Lett. **54**, 1690 (1985).
[14] I. Szleifer *et al.*, Phys. Rev. Lett. **60**, 1966 (1988).
[15] H. Endo *et al.*, Phys. Rev. Lett. **85**, 102 (2000).
[16] B. Jakobs *et al.*, Langmuir **15**, 6707 (1999).
[17] H. Endo *et al.*, J. Chem. Phys. **115**, 580 (2001).
[18] C. Hiergeist and R. Lipowsky, J. Phys. II **6**, 1465 (1996).
[19] P. T. Callaghan and O. Soderman, J. Phys. Chem. **87**, 1737 (1983).
[20] J. Allgaier *et al.*, Macromolecules **30**, 1582 (1997).
[21] A. Poppe *et al.*, Macromolecules **30**, 7462 (1997).
[22] L. J. Fetters and J. W. May, Macromolecules **22**, 921 (1989).
[23] S. Kawaguchi *et al.*, Polymer **38**, 2885 (1997).
[24] V. F. Sears, *Thermal-Neutron Scattering Length and Cross-Sections for Condensed Matter Research* (Chalk River Nuclear Laboratories, Chalk River, Ontario, Canada, 1984).
[25] T. Sottman, R. Strey, and S.-H. Chen, J. Chem. Phys. **15**, 6483 (1997).
[26] *Handbook of Chemistry and Physics*, 57th ed. (CRC, Cleveland, 1976).
[27] R. F. Berg and M. R. Moldover, J. Chem. Phys. **6**, 3687 (1987).
[28] F. Mezei, in *Proceedings of the Workshop on Neutron Spin Echo* (Springer, Berlin, 1980).
[29] M. Monkenbusch, R. Schaetzler, and D. Richter, Nucl. Instrum. Methods Phys. Res. A **399**, 301 (1997).
[30] P. Schleger *et al.*, Physica B **266**, 49 (1999); The ILL Yellow Book, http://www.ill.fr/
[31] A. G. Zilman and R. Granek, Phys. Rev. Lett. **77**, 4788 (1996).
[32] R. Messager *et al.*, J. Phys. (Paris) **51**, 1329 (1990).
[33] For physical reasons, a large-k cutoff in the range $k_{\max}=\pi/a$ exists due to the finite molecular size, which has been assumed in the numerical analysis. However, since the integral is convergent for $k\to\infty$, the influence of $k_{\max}$ is less important.
[34] Zilman and Granek obtain an additional contribution $(k_BT/4\pi\kappa)\ln(\xi/a)$ in ϕ_d, which is inconsistent with a convergent integral in the limit $a\to0$ and $\xi\to\infty$.
[35] F. Brochard and J. F. Lennon, J. Phys. (Paris) **36**, 1035 (1975).
[36] E. Frey and D. R. Nelson, J. Phys. I **1**, 1715 (1991).
[37] G. Gompper *et al.* (to be published).
[38] D. Roux *et al.*, Europhys. Lett. **11**, 229 (1990).
[39] D. Roux, C. Coulon, and M. E. Cates, J. Phys. Chem. **96**, 4174 (1992).
[40] G. Gompper and M. Schick, Phys. Rev. E **49**, 1478 (1994).
[41] R. Granek and M. E. Cates, Phys. Rev. A **46**, 3319 (1992).
[42] S. T. Milner, M. E. Cates, and D. Roux, J. Phys. (France) **51**, 2629 (1990).
[43] G. Gompper and M. Hennes, Phys. Rev. Lett. **73**, 1114 (1994).
[44] M. Hennes and G. Gompper, Phys. Rev. E **54**, 3811 (1996).
[45] M. Nonomura and T. Ohta, J. Chem. Phys. **110**, 7516 (1999).
[46] E. Freyssingeas *et al.*, J. Phys. II **7**, 913 (1997).
[47] S. Ramaswamy *et al.*, Europhys. Lett. **27**, 285 (1994).
[48] T. Schilling, O. Theissen, and G. Gompper, Eur. Phys. J. E **4**, 103 (2001).

[49] For technical reasons, in order to avoid numerical difficulties, the real space upper cutoff was realized by multiplying the integrand with a Gaussian having a width of ξ.
[50] P. N. Pusey and R. J. A. Tough, in *Dynamic Light Scattering-Application of Photon Correlation Spectroscopy*, edited by Robert Pecora (Plenum, New York, 1985).
[51] U. Peter, D. Roux, and A. K. Sood, Phys. Rev. Lett. **86**, 3340 (2001).
[52] A. M. Belloq and G. J. Fuerche, J. Colloid Interface Sci. **78**, 275 (1980).
[53] D. Guest and D. Langevin, J. Colloid Interface Sci. **112**, 208 (1986).
[54] P. G. De Gennes, Physica (Amsterdam) **25**, 825 (1959).
[55] R. Strey, Colloid Polym. Sci. **272**, 1005 (1994).
[56] U. Olson, K. Nagai, and H. Wennerström, J. Chem. Phys. **92**, 6675 (1988).